Revision 1

Scottyite, the natural analogue of synthetic $BaCu_2Si_2O_7$, a new mineral from the Wessels mine, Kalahari Manganese Fields, South Africa

Hexiong Yang[1], Robert T. Downs[1], Stanley H. Evans[1], and William W. Pinch[2]

[1]Department of Geosciences, University of Arizona, Tucson, Arizona 85721-0077, U.S.A.

[2]19 Stonebridge Lane, Pittsford, New York 14534, U.S.A.

Corresponding author: hyang@u.arizona.edu

Abstract

A new mineral species, scottyite, ideally $BaCu_2Si_2O_7$, has been found in the Wessels mine, Kalahari Manganese Fields, Northern Cape Province, South Africa. The mineral appears to have formed as a result of a hydrothermal event and is associated with wesselsite, pectolite, richterite, sugilite, and lavinskyite. Scottyite forms blocky grains with striations parallel to the **c** axis. Crystals are found up to 0.4 x 0.3 x 0.3 mm. No twinning is observed. The mineral is dark-blue in transmitted and under incident lights, transparent with pale blue streak and vitreous luster. It is brittle and has a Mohs hardness of 4~5; cleavage is perfect on {100} and {010} and no parting was observed. The calculated density is 4.654 g/cm^3. Optically, scottyite is biaxial (-), with α =1.750(1), β =1.761(1), and γ =1.765(1), $2V_{meas.}$ = 66(2)º. It is insoluble in water, acetone, or hydrochloric acid. An electron microprobe analysis produced an average composition (wt.%) (8 points) of CuO 36.98(31), BaO 35.12(16), SiO_2 27.01(61), SrO 0.28(5), and Na_2O 0.06(2), and total = 99.45(65), yielding an empirical formula (based on 7 O apfu) $Ba_{1.00}Sr_{0.01}Na_{0.01}Cu_{2.04}Si_{1.97}O_7$.

Scottyite is the natural analogue of synthetic $BaCu_2(Si,Ge)_2O_7$, which exhibits novel one-dimensional quantum spin-1/2 antiferromagnetic properties with tunable super-

exchange interactions. It is orthorhombic, with space group *Pnma* and unit-cell parameters $a = 6.8556(2)$, $b = 13.1725(2)$, $c = 6.8901(1)$ Å, and $V = 622.21(6)$ Å^3. The structure of scottyite is characterized by flattened CuO_4 tetrahedra sharing corners with one another to form chains parallel to the *c* axis. These chains are interlinked by Si_2O_7 tetrahedral dimers and Ba^{2+}. The Ba^{2+} cations are bonded to seven O atoms in a rather irregular coordination. The average Si-O, Cu-O, and Ba-O bond lengths are 1.630, 1.941, and 2.825 Å, respectively. Scottyite is topologically related to a group of compounds with the general formula $BaM^{2+}{}_2Si_2O_7$, where M = Be (barylite and clinobarylite), Fe (andremeyerite), Mg, Mn, Co, and Zn.

***Key words*:** scottyite, $BaCu_2Si_2O_7$, crystal structure, X-ray diffraction, Raman spectra

Introduction

A new mineral species, scottyite, ideally $BaCu_2Si_2O_7$, has been found in the Wessels mine, Kalahari Manganese Fields, Northern Cape Province, Republic of South Africa. It is named after Mr. Michael M. Scott “Scotty", the co-founder and first CEO of Apple Computer Corporation (February 1977 to March 1981), and the founding sponsor of the RRUFF project — an Internet-based, internally-consistent, and integrated database of Raman spectra, X-ray diffraction, and chemistry data for minerals. The vivid color of the mineral reflects his spectroscopic interests, and the synthetic analogue’s high-tech applications mirror his role in introducing the desktop computer to the world. The new mineral and its name have been approved by the Commission on New Minerals, Nomenclature and Classification (CNMNC) of the International Mineralogical Association (IMA 2012-027). Part of the cotype sample has been deposited at the University of Arizona Mineral Museum (Catalogue # 19334) and the RRUFF Project (deposition # R120077). The holotype sample is in the collection of W.W. Pinch.

Silicates with only Ba and Cu as essential structural constituents are relatively rare in nature and only two such minerals have been documented thus far, including effenbergerite $BaCuSi_4O_{10}$ (Giester and Rieck 1994) and scottyite, both originating from the same locality. Nevertheless, Ba-silicate compounds characterized by the general chemical formula $BaM^{2+}{}_2Si_2O_7$ (M^{2+} = Be, Mg, Mn, Fe, Co, Zn, and Cu) have been a subject of extensive investigations for their scientific and industrial interests. For example, the materials with M = Be, Mg, and Zn are suitable hosts for luminescent activating ions. In particular, Pb^{2+}-doped $BaBe_2Si_2O_7$ is used commercially as a UV emitting material in moth-killing lamps and (Eu^{2+} + Mn^{2+})-doped $BaMg_2Si_2O_7$ is a deep-red luminescent emitter through effective energy transfers from Eu^{2+} to Mn^{2+} (Barry 1970; Yao et al. 1998). Moreover, compounds with M = Cu, Co, and Mn are ideal prototypical quasi-one-dimensional quantum spin (=1/2, 3/2, and 5/2, respectively) Heisenberg antiferromagnets with adjustable superexchange interactions, which is vital for our understanding of high-*Tc* superconductivity (e.g., Janczak et al. 1990; Adams and Layland 1996; Lu et al. 2000; Yamada et al. 2001a, 2001b; Ohta et al. 2004a, 2004b; Bertaina and Haya 2006; Zvyagin 2006; Zheludev et al. 2007). Among the $BaM^{2+}{}_2Si_2O_7$ family, the Be- and Fe-bearing members have been found in nature, namely barylite, clinobarylite, and andrémeyerite. This paper describes the physical and chemical properties of scottyite and its crystal structure determined from the single-crystal X-ray diffraction data, demonstrating that scottyite is the natural analogue to the synthetic Cu-member of the $BaM^{2+}{}_2Si_2O_7$ family.

Sample Description and Experimental Methods

Occurrence, physical and chemical properties, and Raman spectra

Scottyite was found on two specimens originating from the central-eastern ore body of the Wessels mine, Kalahari Manganese Fields, Northern Cape Province,

Republic of South Africa. It is in a massive assemblage associated with wesselsite $SrCuSi_4O_{10}$, lavinskyite $K(LiCu)Cu_6Si_8O_{22}(OH)_4$, pectolite $NaCa_2Si_3O_8(OH)$, richterite $Na(CaNa)Mg_5Si_8O_{22}(OH)_2$, and sugilite $KNa_2Fe^{3+}{}_2(Li_3Si_{12})O_{30}$ (Figs. 1 and 2). The mineral assemblage probably formed as a result of a hydrothermal event. Conditions during metamorphism were in the range of 270-420 ºC at 0.2-1.0 kbar (Kleyenstuber 1984; Gutzmer and Beukes 1996). Detailed reviews on the geology and mineralogy of the Kalahari Manganese Fields have been given by Kleyenstuber (1984), Von Bezing et al. (1991), and Gutzmer and Beukes (1996). It should be pointed out that scottyite was actually first reported as an unnamed Ba-Cu silicate from Eifel, Germany (Hentschel 1993; Blaß et al. 2009; Blaß and Schüller 2011). However, this unnamed mineral was not fully described and documented in the list of the IMA valid or invalid unnamed minerals. Since scottyite was approved as a new mineral species based on our mineralogical data, we consider the Wessels Mine, South Africa, rather than Eifel, Germany, as its type locality.

Scottyite forms blocky grains with striations parallel to the **c** axis. Crystals are found up to 0.4 x 0.3 x 0.3 mm. No twinning is observed. The mineral is dark blue, transparent with pale blue streak and vitreous luster. It is brittle and has a Mohs hardness of 4~5; cleavage is perfect on {100} and {010} and no parting was observed. The measured and calculated densities are 4.63(3) and 4.654 g/cm^3, respectively. Optically, scottyite is biaxial (-), with $\alpha = 1.750(1)$, $\beta = 1.761(1)$, $\gamma = 1.765(1)$ (white light), 2V (meas.) = 66(2)º, 2V (calc.) = 62º, and the orientation $X = a$, $Y = b$, $Z = c$. The pleochroism is X = medium blue, Y = dark blue, and Z = medium blue, and the absorption $Y > X = Z$. No dispersion was observed. Scottyite is insoluble in water, acetone, or hydrochloric acid.

The chemical composition was determined using a CAMECA SX-100 electron microprobe (15 kV, 20 nA, < 1 μm beam diameter) (http://rruff.info/scottyite). The standards used included chalcopyrite (Cu), NBS_K458 (Ba), diopside (Si), $SrTiO_3$ (Sr),

and albite (Na), yielding an average composition (wt.%) (8 points) of CuO 36.98(31), BaO 35.12(16), SiO_2 27.01(61), SrO 0.28(5), and Na_2O 0.06(2), and total = 99.45(65). The resultant chemical formula, calculated on the basis of 7 O *apfu* (from the structure determination), is $Ba_{1.00}Sr_{0.01}Na_{0.01}Cu_{2.04}Si_{1.97}O_7$, which can be simplified to $BaCu_2Si_2O_7$.

The Raman spectrum of scottyite was collected on a randomly oriented crystal from 12 scans at 60 s and 100% power per scan on a Thermo Almega microRaman system, using a solid-state laser with a wavelength of 532 nm and a thermoelectric cooled CCD detector. The laser is partially polarized with 4 cm^{-1} resolution and a spot size of 1 μm.

X-ray crystallography

Because of the limited amount of available material, no powder X-ray diffraction data were measured for scottyite. Listed in Table 1 are the powder X-ray diffraction data calculated from the determined structure using the program XPOW (Downs et al. 1993). Single-crystal X-ray diffraction data of scottyite were collected from a nearly equi-dimensional, untwinned crystal (0.04 x 0.05 x 0.05 mm) with frame widths of 0.5° in ω and 30 s counting time per frame. All reflections were indexed on the basis of an orthorhombic unit-cell (Table 2). The intensity data were corrected for X-ray absorption using the Bruker program SADABS. The systematic absences of reflections suggest possible space groups *Pnma* (#62) or $Pn2_1a$ (#33). The crystal structure was solved and refined using SHELX97 (Sheldrick 2008) based on the space group *Pnma*, because it yielded better refinement statistics in terms of bond lengths and angles, atomic displacement parameters, and *R* factors. The positions of all atoms were refined with anisotropic displacement parameters. During the structure refinements, the ideal chemistry was assumed, as the overall effects of the trace amounts of other elements (Sr and Na) on the final structure results are negligible. Final coordinates and displacement

parameters of atoms in scottyite are listed in Table 3, and selected bond-distances in Table 4.

Discussion

Crystal structure

Scottyite is identical with synthetic $BaCu_2Si_2O_7$ (Janczak et al. 1990; Yamada et al. 2001a) and isostructural with $BaCu_2Ge_2O_7$ (Oliveira 1993; Yamada et al. 2001a). Our structure data agree well with those determined for synthetic $BaCu_2Si_2O_7$ by Janczak et al. (1990) using single-crystal X-ray diffraction (Tables 2 and 4). The structure of scottyite is based on a tetrahedral framework consisting of SiO_4 and CuO_4 tetrahedra. The CuO_4 tetrahedra are considerably flattened and share corners to form chains parallel to the **c** axis. The chains are interlinked by the Si_2O_7 dimers oriented parallel to the **b** axis. The Ba^{2+} cations are in the framework channels (Fig. 3). The Cu-O-Cu angle within the CuO_4 tetrahedral chain is 124.49º, which is responsible for the antiferromagnetic coupling in $BaCu_2Si_2O_7$ (Yamada et al. 2001a).

The Ba^{2+} cation in scottyite is bonded to seven O atoms within 3.0 Å in a rather irregular coordination. The next two nearest O atoms (O4) are 3.263 Å away. The bond-valence sum for Ba^{2+}, calculated using the parameters given by Brese and O'Keeffe (1991), is only 1.69 v.u. (Table 5), indicating that it is significantly under-bonded (Table 5). In contrast, the Ba^{2+} cations in effenbergerite are bonded to eight O atoms in a distorted cube coordination with a bond-valence sum of 1.95 u.v. (Chakoumakos et al. 1993; Giester and Rieck 1994). The Cu^{2+} cations in both scottyite and effenbergerite, however, exhibit a similar, nearly planar square coordination. The difference between the Cu coordinations in the two minerals is that the four O atoms bonded to Cu^{2+} in effenbergerite lie in the same plane, with Cu^{2+} slightly (0.67Å) off the plane (Giester and Rieck 1994), whereas they form a markedly flattened tetrahedron in scottyite. The similar planar or nearly planar square coordinations for Cu^{2+} have also been observed in other

synthetic Ba-Cu-silicates, such as *I*-4*m*2 $BaCuSi_2O_6$ (Finger et al. 1989), as well as $I4_1/acd$ and *I*4/*mmm* $BaCuSi_2O_6$ (Sparta and Roth 2004).

The Si-O-Si angle within the Si_2O_7 dimer in scottyite is 134.3º, which is the second largest in the $BaM^{2+}{}_2Si_2O_7$ group, only smaller than that in clinobarylite (138.5º) (Table 6). However, an examination of the clinobarylite structure (Krivovichev et al. 2004) reveals a rather peculiar feature: the $Si\text{-}O_{br}$ (bridging O atom) distance (1.597 Å) is significantly shorter than the $Si\text{-}O_{nbr}$ (non-bridging O atoms) distances (1.619-1.631 Å). This contradicts the previous observations for disilicate compounds (e.g., Lin et al. 1999; Fleet and Liu 2001; Kolitsch et al. 2009), including all other compounds in the $BaM^{2+}{}_2Si_2O_7$ group. Our redetermination of the clinobarylite structure with a crystal from the type locality (Khibiny Massif, Kola Peninsula, Rassia) confirmed its true space group $Pmn2_1$ (R_1 = 0.011 and R_w = 0.026), as that reported by Krivovichev et al. (2004), but yielded the $Si\text{-}O_{br}$ length of 1.657(1) Å and the Si-O-Si angle of 128.82(8)º (Di Domizio et al. 2012). Regardless, the Si-O-Si angles for the compounds in the $BaM^{2+}{}_2Si_2O_7$ group are among the smallest of disilicate materials, which generally exhibit Si-O-Si angles ranging from 120 to 180º (Lin et al. 1999; Fleet and Liu 2001; Kolitsch et al. 2009 and references therein).

There is a strong resemblance in the structural topology among the $BaM^{2+}{}_2Si_2O_7$ compounds, despite their diverse structural symmetries (Table 6): they are all composed of corner-shared MO_4 tetrahedral chains that are interlinked by Si_2O_7 tetrahedral dimers and Ba^{2+} cations. The major differences among these compounds consist in the relative arrangements of Ba^{2+} and Si_2O_7 with respect to the MO_4 tetrahedral chains, thus giving rise to different coordination environments around Ba^{2+} and M^{2+}. For example, the Ba^{2+} cation is only coordinated by five O atoms in high-temperature $Ccm2_1$ $BaZn_2Si_2O_7$, but seven in scottyite, and nine in barylite and clinobarylite. Moreover, there is only one type of symmetrically-distinct MO_4 tetrahedra in scottyite, barylite, clinobarylite, and high-

189 temperature *Ccm*2$_1$ $BaZn_2Si_2O_7$, but two in andrémeyerite, and three in *C*2/*c* compounds
190 in the $BaM^{2+}{}_2Si_2O_7$ group.
191
192 *Raman spectra*
193 The Raman spectrum of scottyite is plotted in Figure 4, along with the spectra of
194 barylite and clinobarylite (R060620 and R060606, respectively, from the RRUFF Project)
195 for comparison. Based on previous experimental and theoretical Raman spectroscopic
196 studies on various disilicate compounds (e.g., Sharma et al. 1988; Fleet and Henderson
197 1997; Makreshi et al. 2007; Kaminskii et al. 2011; Becker et al. 2012), we made a
198 tentative assignment of major Raman bands for scottyite (Table 7). Evidently, the Raman
199 spectra of scottyite, barylite, and clinobarylite are quite similar. In general, they can be
200 divided into four regions. Region 1, between 800 and 1100 cm^{-1}, contains bands
201 attributable to the Si-O symmetric and anti-symmetric stretching vibrations (ν_1 and ν_3
202 modes) within the SiO_4 tetrahedra. Region 2, between 660 and 700 cm^{-1}, includes bands
203 resulting from the Si-O_{br}-Si bending vibrations within the Si_2O_7 tetrahedral dimers. Major
204 bands in region 3, ranging from 420 to 660 cm^{-1}, are ascribed to the O-Si-O symmetric
205 and anti-symmetric bending vibrations (ν_2 and ν_4 modes) within the SiO_4 tetrahedra. The
206 bands in region 4, below 420 cm^{-1}, are mainly associated with the rotational and
207 translational modes of SiO_4 tetrahedra, as well as the Cu-O interactions and lattice
208 vibrational modes.
209 One of the noticeable features in Figure 4 is that the wavenumbers of the bands
210 due to the Si-O_{br}-Si bending mode for barylite and clinobarylite are nearly identical
211 (~685 cm^{-1}), indicating that the Si-O_{br} bond lengths and the Si-O_{br}-Si angles in these two
212 minerals are rather comparable. This is indeed the case. The Si-O_{br} distance and the Si-
213 O_{br}-Si angle are 1.657 Å and 128.59º, respectively, in barylite (Robinson and Fang 1977),
214 and 1.657 Å and 128.82º in clinobarylite (Di Domizio et al. in review). For scottyite, the
215 corresponding band occurs at a wavenumber (674 cm^{-1}) smaller than that for barylite or

clinobarylite. This shift is mostly related to the larger Si-O_{br}-Si angle in scottyite, as the Si-O_{br} bond length in scottyite is identical to that in barylite or clinobarylite. A similar correlation between the positions of the bands stemming from the Si-O_{br}-Si bending vibrations and the Si-O_{br}-Si angles has also been observed in chain silicates with the same or similar structures (Huang et al. 2000 and references therein).

Ba-Sr distribution between scottyite and wesselsite

As shown in Figure 2, scottyite is intimately associated with wesselsite and lavinskyite. The chemical composition of wesselsite in our sample, determined under the same experimental conditions as those for scottyite, is $(Sr_{0.98}Ba_{0.04})_{\Sigma=1.02}Cu_{1.05}Si_{3.97}O_{10}$ (the average of 10 analysis points). Wesselsite is isostructural with effenbergerite ($BaCuSi_4O_{10}$) (Chakoumakos et al. 1993; Giester and Rieck 1994, 1996) and a complete solid solution between them, $(Sr,Ba)CuSi_4O_{10}$, has been observed experimentally (Knight et al. 2010). Very intriguingly, while wesselsite in our sample contains little Ba, scottyite contains essentially no Sr. Thus far, no compound with the composition $SrCu_2Si_2O_7$ has been reported. In fact, there is no documentation for any $SrM_2Si_2O_7$ compounds. It then begs the question whether scottyite in particular and the $BaM_2Si_2O_7$ compounds in general are capable of accommodating a significant amount of smaller Sr^{2+} [The radii of Ba^{2+} and Sr^{2+} in eight-fold coordination are 1.42 and 1.26 Å, respectively (Shannon 1976)]. As described above, the Ba^{2+} cations in the $BaM_2Si_2O_7$ compounds are situated in the cavities in the framework formed by the Si_2O_7 dimers and the MO_4 tetrahedral chains. Conceivably, any substantial replacement of large Ba^{2+} by smaller Sr^{2+} would require, in addition to the other structural adjustments (such as the tilting or distortion of MO_4 and/or SiO_4 tetrahedra), further narrowing of the Si-O-Si angles in the Si_2O_7 dimers in order to better satisfy the bonding environment for Sr^{2+}. This, however, would not be energetically favorable, because the Si-O-Si angles in the $BaM_2Si_2O_7$ compounds are already among the smallest of disilicate materials. For scottyite, the Ba^{2+} cation is

appreciably underbonded (Table 5), suggesting that the current framework is unable to provide it with a tighter bond environment through additional distortion. Accordingly, any sizable substitution of Sr^{2+} for Ba^{2+} would worsen the bonding energetics for this site and thus destabilize the entire structure. Nevertheless, we cannot rule out the possible existence of $SrM_2Si_2O_7$ compounds at different conditions, such as under high pressures.

Acknowledgements

This study was funded by the Science Foundation Arizona.

References Cited

Adams, R.D. and Layland, R. (1996) Syntheses, structural analyses, and unusual magnetic properties of $Ba_2CoSi_2O_7$ and $BaCo_2Si_2O_7$. Inorganic Chemistry, 35, 3492-3497.

Barry, T.L. (1970) Luminescent properties of Eu^{2+} and Eu^{2+} + Mn^{2+} activated $BaMg_2Si_2O_7$. Journal of Electrochemical Society, 117, 381-385.

Becker, P. Libowitzky, E., Bohaty, L., Liebertz, J., Rhee, H., Eichler, H.-J., and Kaminskii, A.A. (2012) Temperature-dependent thermo-mechanical and Raman spectroscopy study of the SRS-active melilite-type crystal $Ca_2ZnSi_2O_7$ (hardystonite) at its incommensurate-commensurate phase transition. Physica Status of Solidi, A209, 327-334.

Bertaina, S. and Hayn, R. (2006) Exchange integrals and magnetization distribution in $BaCu_2X_2O_7$ (X=Ge,Si). Physical Review B, 73, 212409.

Blaβ, G., Graf, H.-W., Kolitsch, U., and Sebold, D. (2009) The new finds from the volcanic Eifel (II). Mineralien-Welt, 20, 38-49. (in German)

Blaβ, G., Schüller, E., and Schüller, W. (2011) „Unglaubliche" Kupfermineralien aus der Vulkaneifel: Auf'm Kopp bei Neroth, Lapis, 22, 21-28, 90. (in German)

Brese, N.E. and O'Keeffe, M. (1991) Bond-valence parameters for solids. Acta Crystallographica, B47, 192–197.

Cannillo, E., Mazzi, F., and Rossi, G. (1988) Crystal structure of andremeyerite, $BaFe(Fe,Mn,Mg)Si_2O_7$. American Mineralogist 73, 608-612.

Chakoumakos, B.C., Fernandez-Baca, J.A., and Boatner, L.A. (1993) Refinement of the structures of the layer silicates $MCuSi_4O_{10}$ (M=Ca,Sr,Ba) by Rietveld analysis of neutron powder diffraction data. Journal of Solid State Chemistry 103, 105-113.

Downs, R.T., Bartelmehs, K.L., Gibbs, G.V. and Boisen, M.B., Jr. (1993) Interactive software for calculating and displaying X-ray or neutron powder diffractometer patterns of crystalline materials. American Mineralogist, 78, 1104-1107.

Finger, L.W., Hazen, R.M., and Hemley, R.J. (1989) $BaCuSi_2O_6$: a new cyclosilicate with four-membered tetrahedral rings. American Mineralogist, 74, 952-955.

Fleet, M.E., and Henderson, G.S. (1997) Structure-composition relations and Raman spectroscopy of high-pressure sodium silicates. Physics and Chemistry of Minerals, 24, 234-355.

Fleet, M.E. and Liu , X. (2001) High-pressure rare earth disilicates $REE_2Si_2O_7$ (REE = Nd, Sm, Eu, Gd): type K. Journal of Solid State Chemistry, 161, 166-172.

Giester, G. and Rieck, B. (1994) Effenbergerite, $BaCu[Si_4O_{10}]$, a new mineral from the Kalahari manganese field, South Africa: description and crystal structure. Mineralogical Magazine, 58, 663-670.

Giester, G. and Rieck, B. (1996) Wesselsite, $SrCu[Si_4O_{10}]$, a further new gillespite-group mineral from the Kalahari Manganese Field, South Africa. Mineralogical Magazine, 60, 795-798.

Gutzmer, J. and Beukes, N.J. (1996) Mineral paragenesis of the Kalahari manganese field, South Africa. Ore Geology Reviews, 11, 405-428.

Hentschel, G. (1993) Die Lavaströme der Graulai: eine neue Fundstelle in der Westeifel. Lapis 12 (9), 11-23. (in German)

297 Huang, E., Chen, C.H., Huang, T., Lin, E.H., and Xu, J.-A. (2000) Raman spectroscopic
298 characteristics of Mg-Fe-Ca pyroxenes. American Mineralogist, 85, 473-479.
299 Janczak, J., Kubiak, R., and Glowiak, T. (1990) Structure of barium copper pyrosilicate
300 at 300 K. Acta Crystallographica, C46, 1383-1385.
301 Kaminskii, A.A., Rhee, H., Lux, O., Eichler, H.J., Bohaty, L., Becker, P., Liebertz, J.,
302 Ueda, K., Shirakawa, A., Voltashev, V.V., Januza, J., Dong, J., and Stavrovskii,
303 D.B. (2011) Many-phonon stimulated Raman scattering and related cascaded and
304 cross-cascaded $\chi^{(3)}$-nonlinear optical effects in melilite-type crystal $Ca_2ZnSi_2O_7$.
305 Laser Physics Letters, 8, 859-874.
306 Kleyenstuber, A.S.E. (1984) The mineralogy of the manganese-bearing Hotazel
307 Formation of the Proterozoic Transvaal sequence of Griqualand West, South
308 Africa. Trans. Geol. Soc. South Africa, 87, 267-275.
309 Knight, K.S., Henderson, C.M.B., and Clark, S.M. (2010) Structural variations in the
310 wesselsite-effenbergerite ($Sr_{1-x}Ba_xCuSi_4O_{10}$) solid solution. European Journal of
311 Mineralogy, 22, 411-423.
312 Kolitsch, U., Wierzbicka-Wieczorek, M., and Tillmanns, E. (2009) Crystal chemistry and
313 topology of two flux-grown yttrium silicates, $BaKYSi_2O_7$ and $Cs_3YSi_8O_{19}$.
314 Canadian Mineralogist, 47, 421-431.
315 Krivovichev, S.V., Yakovenchuk, V.N., Armbuster, T., Mikhailova, Y., Pakhomovsky,
316 Y. A. (2004) Clinobarylite, $BaBe_2Si_2O_7$: structure refinement and revision of
317 symmetry and physical properties. Neues Jahrbuch für Mineralogie, Monatshefte,
318 2004, 373-384.
319 Lin, J.H., Lu, G.X., Du, J., Su, M.Z., Loong, C.-K., and Richardson, J.W., Jr. (1999)
320 Phase transition and crystal structures of $BaZn_2Si_2O_7$. Journal of Physics and
321 Chemistry of Solids, 60, 975-983.
322 Lu, G.X., Yang, L.Q., and Lin, J.H. (2000) One-dimensional magnetic interaction in
323 $BaMn_2Si_2O_7$. Solid State Communications, 114, 113-116.

Makreski, P., Jovanovski, G., Kaitner, B., Gajovic, A., and Biljan, T. (2007) Minerals from Macedonia XVII. Vibrational spectra of some sorosilicates. Vibrational Spectroscopy, 44, 162-170.

Ohta, H., Okubo, S., Inagaki, Y., Hiroi, Z., Kikuchi, H. (2004a) Recent high field ESR studies of low-dimensional quantum spin systems in Kobe. Physica, B346–347, 38–44.

Ohta, H., Okubo, S., Fukuoka, D., Inagaki, Y., Kunimoto, T., Kimata, M., Koyama, K., Motokawa, M., Hiroi, Z. (2004b) Breather excitation observed by high-field ESR in one-dimensional antiferromagnet $BaCu_2(Si_{1-x}Ge_x)_2O_7$ (x=0.65). Journal of Magnetism and Magnetic Materials, 272–276, 929–930.

Oliveira, J.A.S. (1993) Crystal-chemical investigations in the systems CuO-BaO-SiO_2-GeO_2 and BaO-Rh_2O_3. Heidelberger Geowissenschaftliche Abhandlungen, 63, 1-185.

Park, C.-H. and Choi, Y.-N. (2009) Crystal structure of $BaMg_2Si_2O_7$ and Eu^{2+} luminescence. Journal of Solid State Chemistry, 182, 1884-1888.

Robinson, P.D. and Fang, J.H. (1977) Barylite, $BaBe_2Si_2O_7$: its space group and crystal structure. American Mineralogist 62, 167-169

Shannon, R.D. (1976) Revised effective ionic radii and systematic studies of interatomic distances in halides and chalcogenides. Acta Crystallographica, A32, 751–767.

Sharma, S.K., Yoder, Jr., H.S., and Matson, D.W. (1988) Raman study of some melilites in crystalline and glassy states. Geochemica et Cosmochemica Acta, 52, 1961-1967.

Sheldrick, G. M. (2008) A short history of *SHELX*. Acta Crystallographica, A64, 112-122.

Sparta, K.M. and Roth, G. (2004) Reinvestigation of the structure of $BaCuSi_2O_6$ – evidence for a phase transition at high temperature. Acta Crystallographica B60, 491-495.

Von Bezing, K.L., Dixon, R.D., Pohl, D., and Cavallo, G. (1991) The Kalahari

353 Manganese Field, an update. Mineralogical Record, 22, 279-297.
354 Yamada, T., Hiroi, Z., and Takano, M. (2001a) Spin-1/2 Quantum antiferromagnetic
355 chains with tunable superexchange interactions found in $BaCu_2(Si_{1-x}Ge_x)_2O_7$.
356 Journal of Solid State Chemistry, 156, 101-109.
357 Yamada, T., Takano, M., and Hiroi, Z. (2001b) Spin-1/2 quantum antiferromagnetic
358 chains with adjustable superexchange interactions found in $BaCu_2(Si_{1-x}Ge_x)_2O_7$.
359 Journal of Alloys and Compounds, 317–318, 171–176.
360 Yao, G.Q., Lin, J.H., Zhang, L., Lu, G.X., Gong, M.L., and Su, M.Z. (1998) Luminescent
361 properties of $BaMg_2Si_2O_7:Eu^{2+}$, Mn^{2+}. Journal of Materials Chemistry, 8, 585-
362 588.
363 Zheludev, A., Masuda, T., Dhalenne, G., Revcolevschi, A., Frost, C. and Perring, T.
364 (2007) Scaling of dynamic spin correlations in $BaCu_2(Si_{0.5}Ge_{0.5})_2O_7$. Physical
365 Review B, 75, 054409.
366 Zvyagin, A.A. (2006) Effect of doping on the magnetic ordering of quasi-one
367 dimensional antiferromagnets. Low Temperature Physics, 32, 158-161.
368
369
370
371

List of Tables

List of Figure Captions


R120077
1 cm

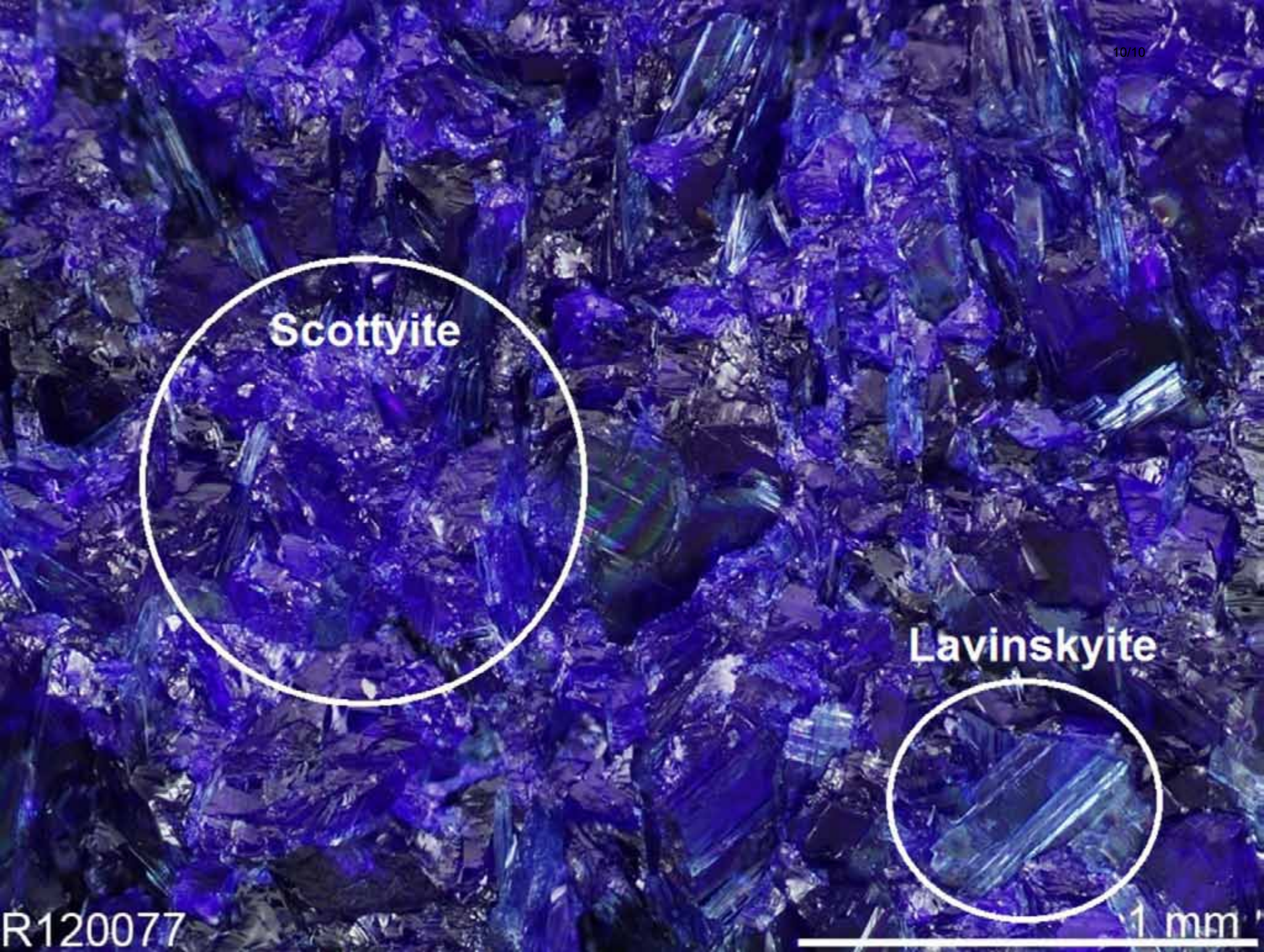
Scottyite
Lavinskyite
R120077
1 mm

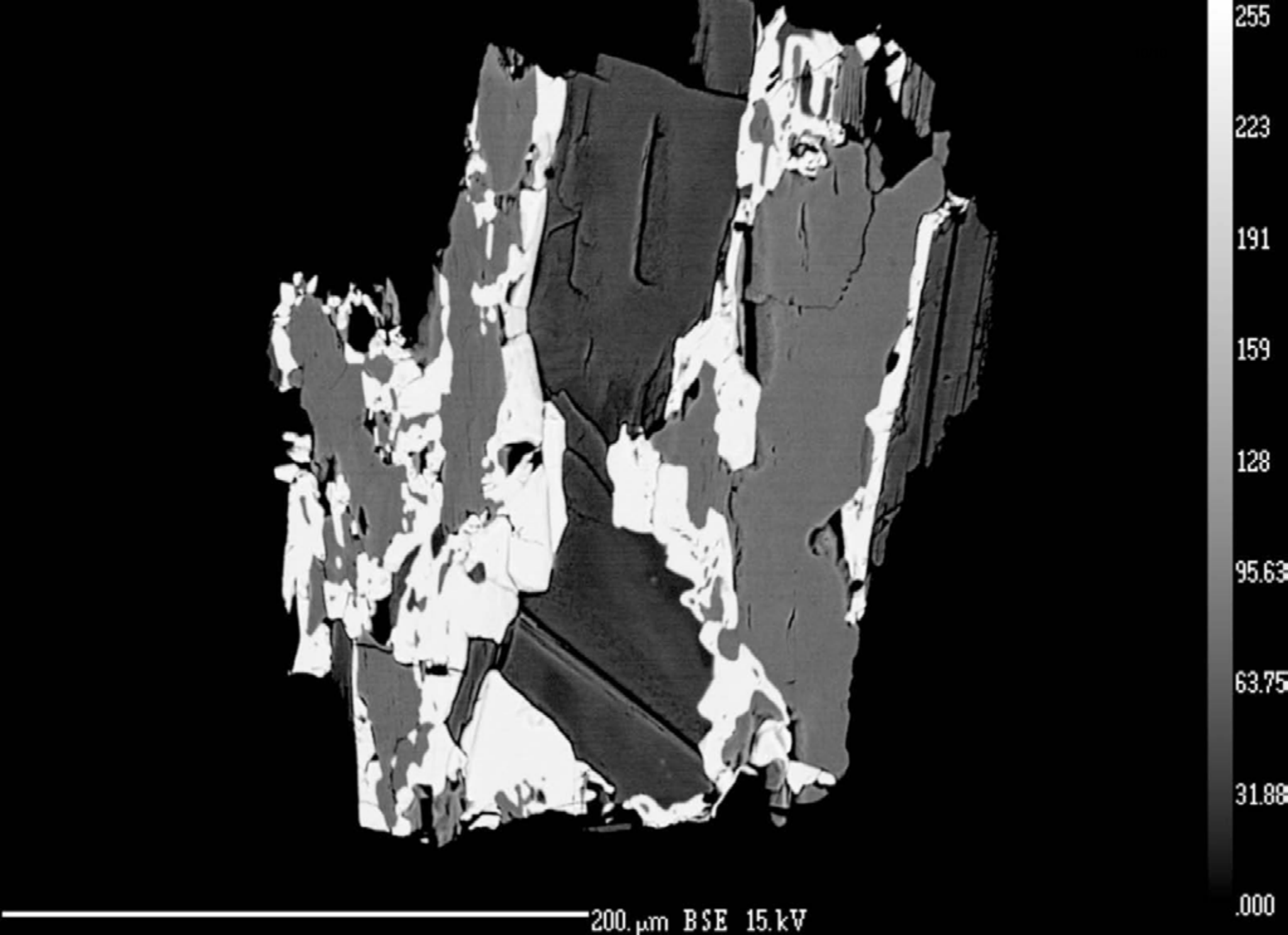
255
223
191
159
128
95.63
63.75
31.88
.000
200.μm BSE 15.kV

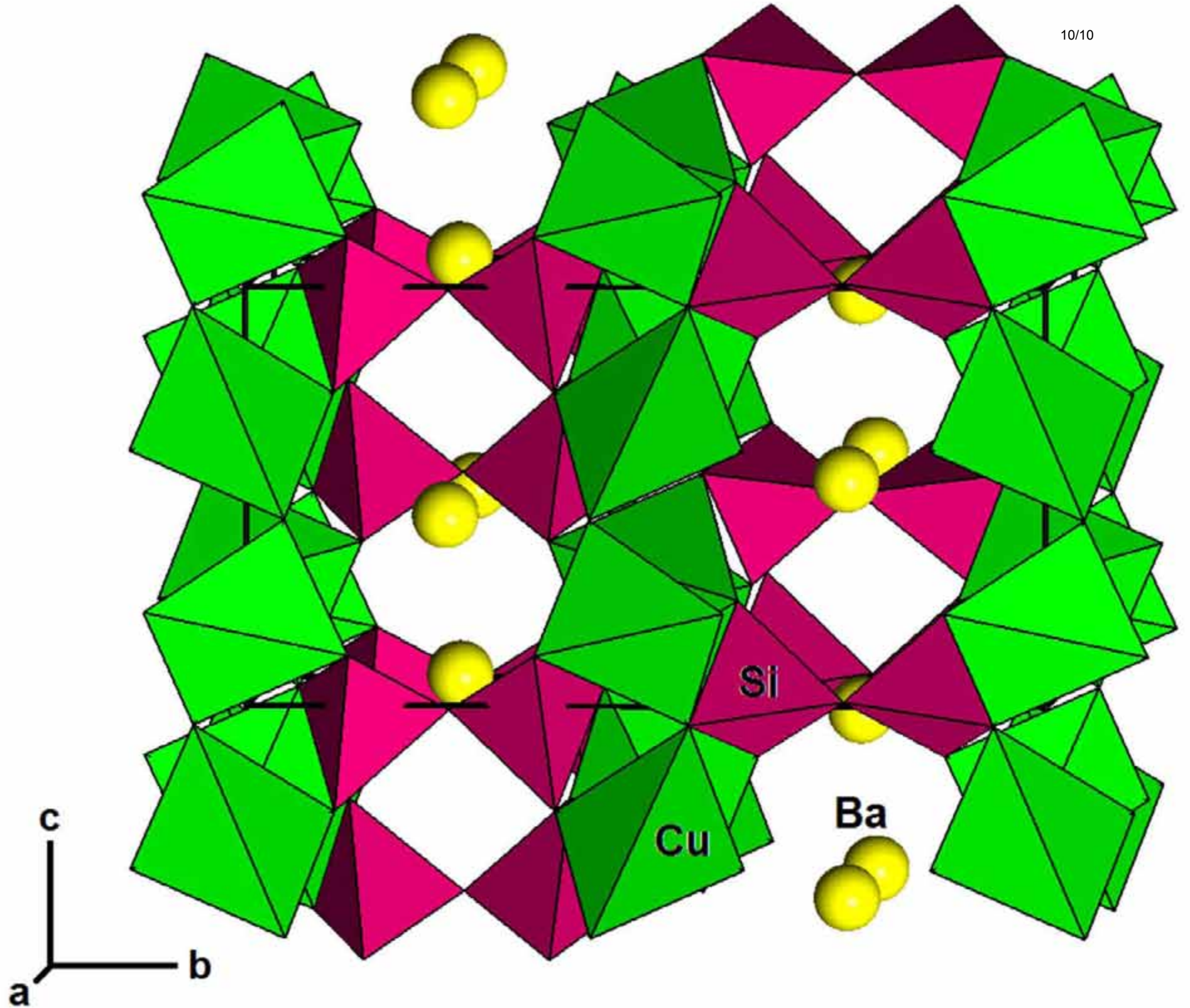
Si
Cu
Ba
c
b
a

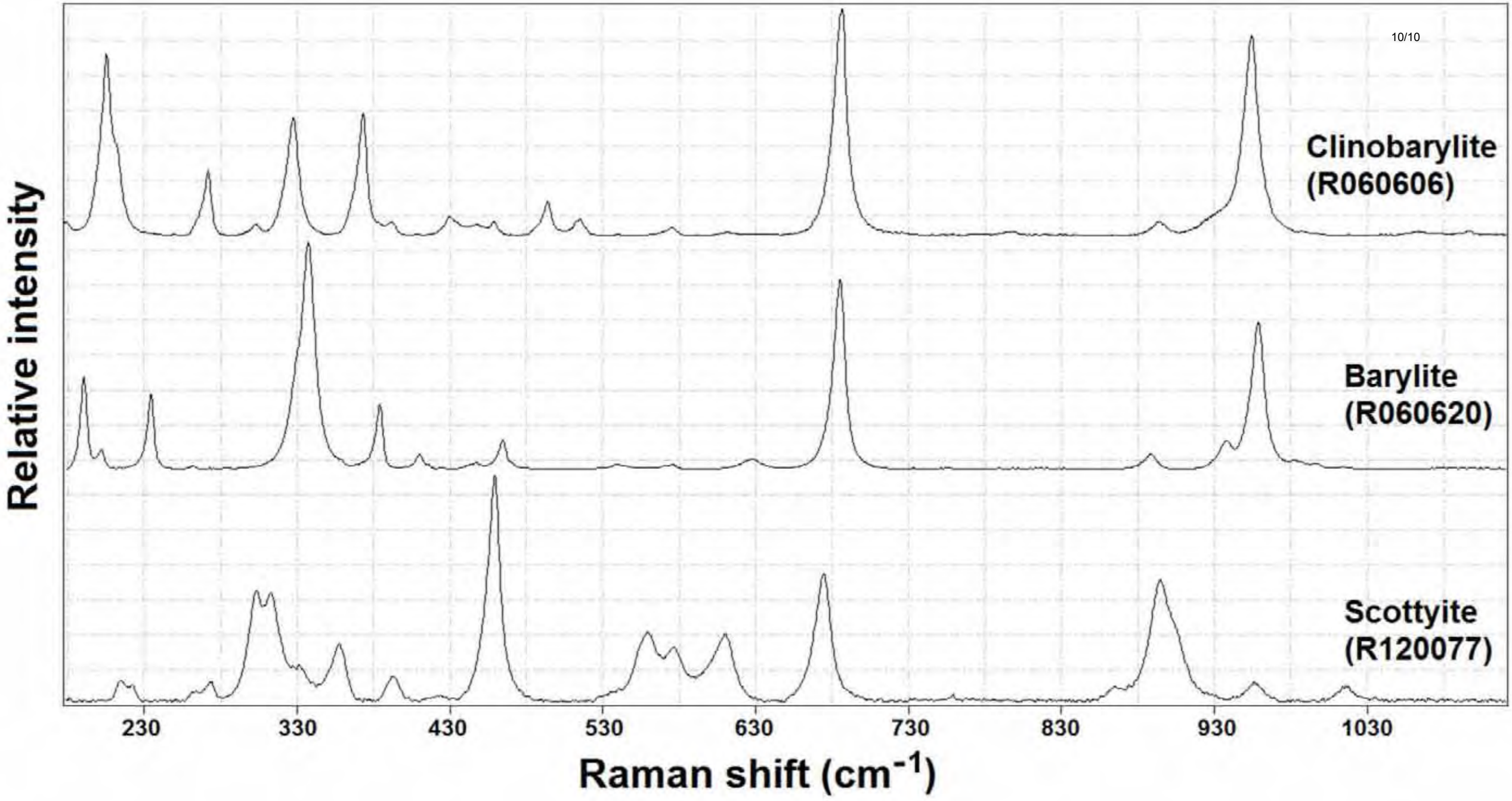
Clinobarylite
(R060606)
Barylite
(R060620)
Scottyite
(R120077)
Relative intensity
230
330
430
530
630
730
830
930
1030
Raman shift (cm-1)

Table 1. Calculated powder X-ray diffraction data for scottyite

Intensity	$d_{calc.}$	h	k	l
51.70	**6.5862**	**0**	**2**	**0**
1.46	6.1053	0	1	1
4.92	4.8598	1	0	1
21.96	**3.9105**	**1**	**2**	**1**
1.50	3.7029	0	3	1
2.03	3.3173	2	1	0
10.74	3.2931	0	4	0
16.92	3.0782	1	0	2
5.41	3.0690	2	0	1
63.84	**3.0527**	**0**	**2**	**2**
100.00	**3.0406**	**2**	**2**	**0**
5.41	2.9975	1	1	2
2.09	2.9889	2	1	1
12.31	2.7887	1	2	2
11.74	2.7818	2	2	1
51.65	**2.7262**	**1**	**4**	**1**
3.38	2.5205	1	3	2
10.71	2.5154	2	3	1
1.94	2.4608	0	5	1
37.15	**2.4299**	**2**	**0**	**2**
1.05	2.3896	2	1	2
5.44	2.3805	0	4	2
16.44	2.3748	2	4	0
4.61	2.3161	1	5	1
1.56	2.2797	2	2	2
3.74	2.2626	0	1	3
2.99	2.2488	1	4	2
2.95	2.2452	2	4	1
1.42	2.1954	0	6	0
1.18	2.1690	3	0	1
1.96	2.1486	1	1	3
2.15	2.1261	2	3	2
2.02	2.0888	2	5	0
4.78	2.0676	1	2	3
4.27	2.0602	3	2	1
5.06	2.0007	1	6	1
20.52	**1.9552**	**2**	**4**	**2**
1.20	1.9510	1	3	3
2.18	1.9080	2	0	3
2.43	1.9043	3	0	2
5.18	1.8847	3	1	2
12.93	1.8514	0	6	2
15.11	1.8487	2	6	0

2.53	1.8294	3	2	2
3.04	1.8165	1	4	3
5.90	1.8114	3	4	1
6.35	1.7874	1	6	2
2.24	1.7499	2	3	3
4.88	1.7225	0	0	4
7.82	1.7139	4	0	0
6.96	1.6706	1	0	4
4.51	1.6573	1	1	4
2.72	1.6485	3	4	2
11.99	1.6466	0	8	0
4.77	1.6290	2	6	2
10.00	1.6193	1	2	4
3.70	1.6126	4	2	1
1.18	1.5614	1	3	4
2.11	1.5461	1	6	3
2.64	1.5453	2	5	3
5.94	1.5430	3	6	1
2.92	1.5203	4	4	0
4.65	1.4987	2	2	4
9.34	1.4945	4	2	2
6.31	1.4899	1	4	4
7.26	1.4846	4	4	1
1.11	1.4556	0	7	3
10.60	1.4536	3	4	3
3.65	1.4519	1	8	2
1.19	1.4386	3	6	2
3.42	1.3943	2	4	4
2.79	1.3909	4	4	2
1.63	1.3755	3	0	4
2.46	1.3681	3	1	4
14.20	1.3631	2	8	2
4.20	1.3465	3	2	4

Table 2. Summary of crystal data and refinement results for scottyite and synthetic $BaCu_2Si_2O_7$.

	Scottyite	synthetic $BaCu_2Si_2O_7$
Ideal chemical formula	$BaCu_2Si_2O_7$	$BaCu_2Si_2O_7$
Crystal symmetry	Orthorhombic	Orthorhombic
Space group	*Pnma* (#62)	*Pnma* (#62)
a(Å)	6.8556(2)	6.866(2)
b(Å)	13.1725(2)	13.190(3)
c(Å)	6.8901(1)	6.909(2)
V(Å^3)	622.21(6)	627.7(3)
Z	4	4
ρ_{cal}(g/cm^3)	4.654	4.592
λ (Å, Mo$K\alpha$)	0.71073	0.71069
μ (mm^{-1})	13.41	13.75
2θ range for data collection	≤65.12	60.0
No. of reflections collected	4887	
No. of independent reflections	1180	
No. of reflections with $I > 2\sigma(I)$	1065	1039
No. of parameters refined	59	59
R(int)	0.023	0.028
Final R_1, wR_2 factors [$I > 2\sigma(I)$]	0.017, 0.040	0.031, 0.037
Final R_1, wR_2 factors (all data)	0.021, 0.041	
Goodness-of-fit	1.074	
Reference	This study	Janczak et al. (1990)

Table 3. Coordinates and displacement parameters of atoms in scottyite

Atom	*x*	*y*	*z*	U_{eq}	U_{11}	U_{22}	U_{33}	U_{23}	U_{13}	U_{12}
Ba	0.01303(2)	1/4	0.45688(3)	0.00970(5)	0.0089(1)	0.0108(1)	0.0095(1)	0	-0.0008(1)	0
Cu	0.27762(4)	0.00417(2)	0.20631(4)	0.00714(6)	0.0089(1)	0.0057(1)	0.0068(1)	-0.0008(1)	-0.0023(1)	0.0014(1)
Si	0.49765(7)	0.13406(5)	0.52716(8)	0.0057(1)	0.0066(2)	0.0047(2)	0.0057(3)	-0.0000(2)	0.0004(2)	0.00039(2)
O1	0.4044(3)	1/4	0.5167(3)	0.0087(4)	0.0084(9)	0.0057(9)	0.0120(9)	0	-0.0004(8)	0
O2	0.1725(2)	0.1337(1)	0.1306(2)	0.0104(3)	0.0122(6)	0.0068(7)	0.0122(7)	-0.0003(6)	-0.0053(6)	0.0022(5)
O3	0.5590(2)	0.1121(1)	0.7486(2)	0.0111(3)	0.0152(7)	0.0098(7)	0.0083(7)	-0.0017(6)	-0.0031(6)	0.0048(6)
O4	0.3173(2)	0.0596(1)	0.4658(2)	0.0078(3)	0.0105(6)	0.0076(7)	0.0053(6)	-0.0010(5)	0.0007(5)	-0.0022(5)

Table 4. Selected bond distances in scottyite and synthetic $BaCu_2Si_2O_7$.

	Scottyite	synthetic $BaCu_2Si_2O_7$
	Distance (Å)	Distance (Å)
Ba-O1	2.715(2)	2.713(5)
-O2 x2	2.857(2)	2.863(3)
-O2 x2	2.932(2)	2.932(3)
-O3	2.741(2)	2.749(3)
Ave.	2.825	2.830
Cu-O2	1.924(2)	1.930(3)
-O3	1.923(2)	1.926(2)
-O4	1.950(2)	1.956(2)
-O4	1.968(2)	1.973(3)
Ave.	1.941	1.946
Si-O1	1.657(1)	1.662(2)
-O2	1.618(2)	1.619(4)
-O3	1.609(2)	1.610(4)
-O4	1.634(2)	1.635(3)
Ave.	1.630	1.632

Table 5. Calculated bond-valence sums for scottyite.

	O1	O2	O3	O4	Sum
Ba	0.317	0.216×2→ 0.176×2→	0.296×2→		1.693
Cu		0.516	0.517	0.481 0.458	1.972
Si	0.915×2↓	1.016	1.041	0.973	3.945
Sum	2.147	1.924	1.854	1.912	

Table 6. Comparison of crystallographic data for $BaM_2Si_2O_7$-type minerals and compounds

	Chemical formula	S.G.	Unit-cell parameters				Si-O-Si (º)	Ba-coordination	Reference
			a (Å)	*b*(Å)	*c*(Å)	β(º)			
Scottyite	$BaCu_2Si_2O_7$	*Pnma*	6.8556	13.1725	6.8901		134.3	7	(1)
Barylite	$BaBe_2Si_2O_7$	*Pnma*	9.820	11.670	4.690		128.6	9	(2)
Clinobarylite	$BaBe_2Si_2O_7$	$Pmn2_1$	11.650	4.922	4.674		138.5	9	(3)
Clinobarylite	$BaBe_2Si_2O_7$	$Pnm2_1$	4.9175	11.6491	4.6746		128.8	9	(1)
Andremeyerite	$BaFe_2Si_2O_7$	$P2_1/c$	7.488	13.785	7.085	118.23	127.2	7	(4)
Synthetic	$BaCo_2Si_2O_7$	*C*2/*c*	7.2131	12.781	13.762	90.299	124.5	8	(5)
Synthetic	$BaMg_2Si_2O_7$	*C*2/*c*	7.2455	12.7138	13.7481	90.211	125.2	7	(6)
Synthetic	$BaMn_2Si_2O_7$	*C*2/*c*	7.2953	12.9632	14.0321	90.248	no data		(7)
Synthetic	$BaZn_2Si_2O_7$-25°C	*C*2/*c*	7.2782	12.8009	13.6869	90.093	124.8	8	(8)
Synthetic	$BaZn_2Si_2O_7$-280 °C	$Ccm2_1$	7.6199	13.0265	6.7374		131.7	5	(8)

References: (1) This work; (2) Robinson and Fang (1977); (3) Krivovichev et al. (2004); (4) Cannillo et al. (1988); (5) Adams and Layland (1996); (6) Park and Choi (2009); (7) Lu et al. (2000); (8) Lin et al. (1999).

Note: The *a* and *b* axis for clinobarylite were switched in our structure refinement to facilitate a direct comparison with the unit-cell setting for barylite.

Table 7. Tentative assignments of major Raman bands for scottyite

Bands (cm^{-1})	Intensity	Assignment
1019, 958, 866	Relatively weak	ν_3 (SiO_4) anti-symmetric stretching
896	Strong, sharp	ν_1 (SiO_4) symmetric stretching
675	Strong, sharp	Si-O-Si bending
612, 578, 560	Relatively strong, sharp	ν_4 (SiO_4) anti-symmetric bending
459	Very strong, sharp	ν_2 (SiO_4) symmetric bending
<420	Strong to weak	SiO_4 rotational modes, lattice vibrational modes, and Cu-O interactions